Eur. Phys. J. D **23**, 375–383 (2003)
DOI: 10.1140/epjd/e2003-00091-y

THE EUROPEAN PHYSICAL JOURNAL D

Isomerization and dissociation of small $(CH_3CN)_n$ molecular clusters: a computational study

P. Parneix[a]

Laboratoire de Photophysique Moléculaire[b], CNRS, bâtiment 210, Université de Paris-Sud, 91405 Orsay Cedex, France

Received 19 November 2002 / Received in final form 5 February 2003
Published online 29 April 2003 –

Abstract. The isomerization and evaporation processes in the neutral homogeneous $(CH_3CN)_n$ molecular clusters ($n = 2-7$) have been investigated using classical molecular dynamics simulations. The evaporation rate constants and the kinetic energy release in the dissociation have been analysed as a function of the cluster size and as a function of the internal energy in the parent cluster. The competition between monomer and dimer ejections has been also carefully studied. All the dynamical properties in these dissociative processes have been discussed in relation to the static properties of the clusters involved in the dissociation and also in relation to the solid-liquid like transition which appears in these homogeneous molecular clusters.

PACS. 36.40.Ei Phase transitions in clusters – 36.40.Qv Stability and fragmentation of clusters

1 Introduction

Due to their large dipole moment, the interaction between acetonitrile molecules is largely influenced by strong dipole-dipole forces. In acetonitrile liquids, both neutron scattering and X-ray experimental studies have clearly shown some specific orientational behaviours with a short range order due to the strong dipole-dipole interaction [1,2]. In bulk acetonitrile solids, the crystalline arrangement of the molecules has also been analysed under different temperature conditions. At low temperature, a structure with paired parallel dipoles, called the α phase, has been experimentally evidenced [3].

Far IR spectroscopy has been used to characterize the anti-parallel structure of the acetonitrile dimer embedded in an inert gas matrix [4,5]. Diffraction studies have also allowed the observation of the antiparallel configuration for the dimer in liquid matrices [6]. Information on the geometry of the free $(CH_3CN)_n$ molecular clusters has also been obtained from IR-photodissociation [7–12] and much more recently from IR-photodissociation of acetonitrile clusters embedded in cold helium droplets [13]. Recently the electron photodetachment technique has been used in order to extract information on mass-selected clusters [14].

From a theoretical point of view, different intermolecular semi-empirical potentials have been developed over the last few years. The first one was proposed by Evans [15] and the same year a potential model was proposed by Böhm *et al.* [16] in which the electrostatic interaction was reproduced by point charges located on the 6 atoms of the molecule. From this parametrization the dipole moment was found to be 4.14 D compared to the experimental value of 3.91 D [17]. Later an OPLS (optimized potential for liquid simulation) has been developed by Jorgensen *et al.* [18] in which only 4 point charges were used, allowing a decrease of the computational time. However within this new parametrization, the calculated dipole moment was only 3.44 D. Much more recently, an *ab initio* calculation (MP2 level) has been performed for the $(CH_3CN)_n$ acetonitrile clusters up to $n = 4$ [19,20].

By using the semi-empirical potentials, structure calculations have been performed [21,22]. Isomerization dynamics and thermodynamical properties of the $(CH_3CN)_n$ clusters have been also analysed from classical microcanonical [23,24] or canonical [25] simulations. As expected, the calculated properties have been found to be very sensitive to the odd/even character of the number of molecules inside the cluster. In particular, the melting temperature associated with the solid-liquid like transition is dramatically dependent on the number of molecules n (the melting temperature was found higher when n is even than when n is odd).

This typical evolution of the molecular cluster properties *versus* the cluster size and the strong trend to dimerize inside the cluster, has led us to be interested in the simulation of the evaporation dynamics in such a system which can be considered as a model system for the analysis of the competition between the ejection of a monomer and a dimer from an initially highly vibrationally excited parent cluster. Up to now, the simulation of the evaporation dynamics has been mainly studied in the case of

[a] e-mail: pascal.parneix@ppm.u-psud.fr
[b] Laboratoire associé à l'université Paris-Sud.

van der Waals atomic clusters [26–30] or metallic atomic clusters [31–33]. Only very few studies have analysed the dissociation dynamics in molecular clusters [34–36]. Some of these theoretical studies have given evidence of the influence of the solid-liquid like transition in the product clusters on the evolution of the evaporation rates and the mean kinetic energy release *versus* the internal energy in the parent cluster [29,30,34–36]. Such a sensitivity of the evaporation dynamics to the thermodynamical phase of the cluster has been first established by using the classical Phase Space Theory statistical approach [29].

In this context, the present study is devoted to the analysis of the possible effect of the solid-liquid like transition on the evaporation dynamics and particularly on the competition between the monomer and dimer evaporation as a function of the internal energy. Experimental characterizations of the solid-liquid like transitions could then be relatively easily achieved from time-of-flight experiments.

The paper is organized as follows: a first section will be devoted to the description of the simulation methods while the results will be discussed in a second section.

2 Methodology and numerical procedure

2.1 Potential model

Different potential models have been proposed in the recent past to describe the interaction between acetonitrile molecules. To make the comparison with previous theoretical studies on the equilibrium configurations of these clusters but also on the isomerization dynamics, I have considered the analytic potential model which has been proposed by Böhm *et al.* [16], first developed to reproduce the properties of liquid acetonitrile. In this approach, the electrostatic interaction between the polar molecules is described by considering 6 point charges localized on each atom of the rigid molecule. The charges were deduced from an *ab initio* RHF calculation with a 6-31G** atomic basis. From this electrostatic potential, another contribution is added which describes the van der Waals interaction between the molecules. A sum of Lennard-Jones atom-atom potentials between all the atoms of each molecule is then used. The analytic form of the total intermolecular potential between two molecules can be thus summarized by:

$$V = \sum_{i=1}^{6} \sum_{j>i} \left\{ \frac{e^2}{4\pi\epsilon_0} \frac{q_i q_j}{r_{ij}} + 4\epsilon_{ij} \left[\left(\frac{\sigma_{ij}}{r_{ij}} \right)^{12} - \left(\frac{\sigma_{ij}}{r_{ij}} \right)^{6} \right] \right\} \tag{1}$$

r_{ij} corresponds to the distance between the ith and the jth atoms. All the potential parameters are reported in Table 1. In this table, C_1 and C_2 respectively correspond to the carbon atoms in the methyl and cyanide groups. The combination rules have been used to obtain the σ and ϵ parameters for the interaction between heterogeneous atoms:

$$\epsilon_{ij} = \sqrt{\epsilon_{ii}\epsilon_{jj}}$$

$$\sigma_{ij} = \frac{\sigma_{ii} + \sigma_{jj}}{2}. \tag{2}$$

Table 1. Potential parameters for the empirical intermolecular potential between two CH_3CN molecules.

Atom	Q $\lvert e\rvert$	σ (Å)	(ϵ) (kJ mole^{-1})
C_1 (CH_3 site)	−0.577	3.0	0.4177
C_2 (CN site)	+0.488	3.4	0.4177
N	−0.514	3.3	0.4177
H	0.201	2.2	0.0835

All these potential parameters were adapted for a given rigid geometry of the molecules. The C_1C_2, C_2N, C_1H and HH distances were respectively equal to 1.460, 1.170, 1.087 and 1.771 Å. The angle HC_1C_2 was equal to 109.8 degrees.

It has to be mentioned here that other potentials have been used in the litterature, leading to a change in the topology of the potential energy surface. Consequently a direct comparison with experiments is not at all obvious. This study has to be much more considered as a modelisation of the evaporation dynamics for a model cluster with polar molecules.

2.2 Molecular dynamics simulation

The dynamics of the $(CH_3CN)_n$ cluster has been studied using molecular dynamics (MD) simulations in the microcanonical ensemble by integrating Hamilton's equations to generate classical trajectories in phase space. Classical trajectories were numerically propagated using a standard fourth and fifth order predictor-corrector algorithm for the rotation and translation, respectively. The acetonitrile molecule was described as a rigid body and the quaternion formalism [38] was used to describe its rotation in space. The integration time step was equal to 0.5 fs and the energy conservation was equal to around 0.001%. All the simulations were performed with the total angular momentum $\mathbf{J} = \mathbf{0}$.

2.2.1 MD simulation of the isomerization dynamics

The isomerization dynamics has been analysed along constant energy trajectories whose duration was equal to 50 ns after an equilibration time of 200 ps.

The kinetic temperature for the non-rotating cluster was calculated from the expression:

$$T = \frac{2\langle E_{\mathrm{k}} \rangle}{(6n-6)k_{\mathrm{B}}}.$$

In this last equation, n corresponds to the number of rigid CH_3CN molecules and $\langle E_{\mathrm{k}} \rangle$ is the time average of the kinetic energy and k_{B} the Boltzman's constant.

The rigidity of the clusters has been analysed from the fluctuations of the intermolecular distance as a function of time. Quantitative information on these distance fluctuations in a $(CH_3CN)_n$ cluster has been obtained with the

usual procedure, *i.e.* by calculating the root mean square amplitude δ given by:

$$\delta = \frac{2}{n(n-1)} \sum_{i=1}^{n} \sum_{j>i} \frac{\sqrt{\langle r_{ij}^2 \rangle - \langle r_{ij} \rangle^2}}{\langle r_{ij} \rangle}.$$

In this expression $\langle r_{ij} \rangle$ corresponds to the time-averaged distance between the ith and the jth molecules. It is generally admitted that a liquid-like behaviour of the clusters can be characterized when δ becomes larger than approximately 0.1.

2.2.2 MD simulation of the evaporation dynamics

The dissociation dynamics has been also investigated from classical MD simulations. In the first step of the simulation, the clusters were initially prepared with a high kinetic temperature ($T = 100-150$ K) allowing an efficient communication between all isomeric forms. From this procedure, a large volume of the phase space was accessible during this first trajectory. However, the internal vibrational energy was not large enough to induce dissociation of the cluster within a time of about 50 ns. Along this first trajectory, initial conditions for an ensemble of evaporative trajectories were generated each 2.5 ps by scaling the linear and angular momenta to obtain the desired energy value E. For each energy, 2000 dissociative trajectories were thus generated which allowed reliable averaged values in the microcanonical ensemble to be obtained.

The evaporative trajectories were stopped when one molecule was found at a distance larger than $R_c = 30$ Å and the evaporation time was taken as the last time for which the radial velocity of the center of mass of the molecule was negative. This dynamical definition of the time of evaporation prevents this time depending on the release kinetic energy of the fragments in the dissociation. If the evaporation time was less than 5 ps, the event was rejected to avoid trajectories for which statistical redistribution of the internal energy in the cluster was not yet achieved before dissociation.

For the $(CH_3CN)_n$ clusters with $n = 4$ and 5, two dissociative channels were opened in the energy regime considered in this study. It corresponds to the evaporation of one (monomer) or two molecules (dimer) from the initial hot cluster. In the MD simulations, a geometrical criterium was used to discriminate between these two channels: if the distance between the evaporated molecule and one other molecule was less than 8 Å, the product was considered as a dimer. The maximum duration of each individual dissociative trajectory was equal to 5 ns. The branching ratio was directly determined as the ratio of the number of trajectories involving respectively monomer and dimer evaporations. For each internal energy, 10 sets of 200 trajectories have been considered in order to estimate the uncertainty from the student's statistical approach employing a student's coefficient confidence of 95%.

The global evaporation rate constant k_e was calculated from the linear fit of the $\ln[N(t)/N(t=0)]$ curve in which $N(t)$ correspond to the number of clusters not yet dissociated at time t. The specific evaporation rate constants $k_{e,m}$ and $k_{e,d}$ respectively for the monomer and dimer evaporation are just given by $k_{e,m} = p_1 k_e$ and $k_{e,d} = p_2 k_e$ in which p_1 and p_2 are respectively the probabilities to obtain a monomer and a dimer in the evaporation process. When only these two evaporative channels are opened, the two probabilities are obviously linked by $p_2 = 1 - p_1$.

From the MD trajectories, information about the energetics of the fragmentation could also be extracted. Consider first the case of the monomer ejection from the hot parent molecular cluster. The translational kinetic energy of the fragments, $\epsilon_{tr}^{(1)}$, was calculated from:

$$\epsilon_{tr}^{(1)} = \frac{\mathbf{P}_1^2}{2\mu_1} \tag{3}$$

where $\mathbf{P}_1$ is the linear momentum of the evaporated CH_3CN molecule expressed in the whole cluster center of mass frame, and μ_1 is the reduced mass of the $CH_3CN + (CH_3CN)_{n-1}$ system.

When the trajectory is stopped, the distance between the monomer and the sub-cluster is large enough that the interaction potential between the two fragments has become very weak. Consequently the rotational energy $\epsilon_{rot}^{(1)}$ is effectively constant and can be easily calculated. The rovibrational energy of the sub-cluster $(CH_3CN)_{n-1}$ following the dissociation could thus be deduced from:

$$E_{rovib}^{(SC)} = E - \epsilon_{tr}^{(1)} - \epsilon_{rot}^{(1)} - E_0. \tag{4}$$

In this last expression E_0 (>0) corresponds to the energy difference between the most stable parent and product clusters.

In the case of the dimer evaporation, the translational kinetic energy release was obtained from equation (5) by taking now the reduced mass of the $(CH_3CN)_2 + (CH_3CN)_{n-2}$ system. From the knowledge of the rotational energy of each individual molecules in the dimer, from the interaction potential energy between the two molecules and from the vibrational energy in the dimer, its rovibrational energy has been deduced. Following the scheme previously described, the rovibrational energy of the sub-cluster has been thus calculated.

3 Results and discussion

3.1 Isomer configuration and isomerization process

Within the potential energy surface (PES), the minimum energy configurations have been calculated for the small clusters ($n = 2-5$) from a quenching procedure. For each cluster size, the binding energies of the most stable isomer has been reported in Table 2. These results are in perfect agreement with the previous calculations realized with the same intermolecular potential model [16, 22].

Table 2. Calculated binding energies and melting temperatures for the most stable $(CH_3CN)_n$ clusters up to $n = 5$.

Number of molecules	Energy (cm^{-1})	$T_{melting}$ (K)
2	−1936	220
3	−3750	28
4	−6896	153
5	−8606	32

For the dimer cluster, only one isomer has been found whose minimum energy structure corresponds to an antiparallel configuration. This structure naturally allows a minimization of the strong electrostatic dipole-dipole interaction. The binding energy in such a configuration is equal to $-1\,936$ cm^{-1} with an intermolecular distance equal to 3.44 Å.

For larger clusters, many minima in the potential energy surface have been characterized. For the $n = 3$ cluster, the most stable isomer corresponds to a C_{3h} structure whose binding energy is equal to $-3\,750$ cm^{-1}. However it has to be noted the presence of two other local minima with only a slightly smaller value of the binding energy, *i.e.* $-3\,718$ and $-3\,678$ cm^{-1} which could be formed in the dissociative process of the $(CH_3CN)_4$ cluster.

For the $(CH_3CN)_4$ cluster, the most stable configuration corresponds to a S_4 geometry in which two dimers are in an anti parallel configuration but with a dimer rotated by 90 degrees with respect to the other. The binding energy of this structure is equal to $-6\,896$ cm^{-1}. The analysis of the quenching trajectories for the tetramer $(CH_3CN)_4$ cluster has revealed that the population in a less stable D_{2d} symmetry isomer ($E = -6\,662$ cm^{-1}) is relatively large (about 20%) which indicates that this metastable isomer should have an important role in the dynamics of this $n = 4$ cluster. Finally the most stable isomer for the pentamer can be viewed as a stable S_4 tetramer on which a fifth molecule is attached.

The isomerization dynamics in homogeneous $(CH_3CN)_n$ clusters has been also investigated both from microcanonical [23] and canonical [25] simulations. These authors have clearly shown evidence for the strong dependence of the melting temperature with the odd/even character of the number of molecules. As I was mainly interested in the relationship between the evaporation dynamics and the solid-liquid like transition, we have run very long MD trajectories (50 ns) in order to obtain some precise values of the melting temperatures for small $(CH_3CN)_n$ clusters.

In Figure 1, the root-mean square amplitudes δ [see Eq. (4)] and the kinetic temperature [see Eq. (3)] have been plotted as a function of the energy for $n = 3$, 4 and 5. It appears clearly that the melting temperature is significantly higher for $n = 4$ than for $n = 3$ or 5. The melting temperatures for $n = 2{-}5$ are summarized in Table 2 and these values are in quite good agreement with the melting temperatures previously calculated by Del Mistro and Stace [23] with the same PES but with shorter MD trajectories.

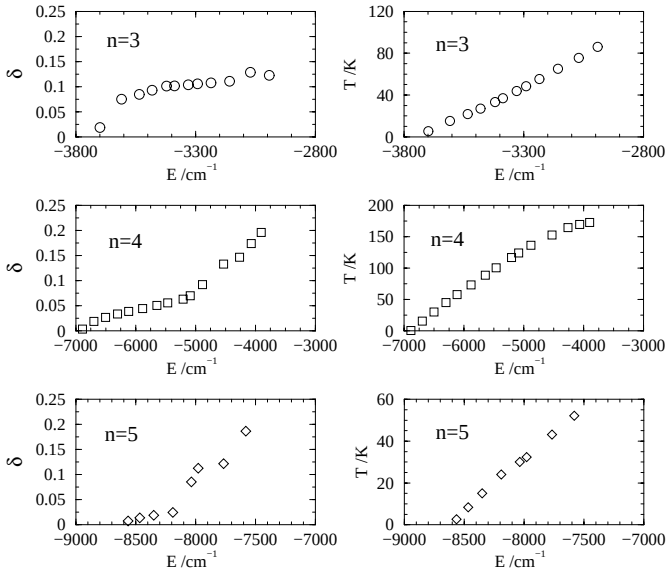

Fig. 1. Plot of the kinetic temperature T and the root-mean square amplitude δ as a function of the internal energy per molecule E/n for $n = 3$, 4 and 5.

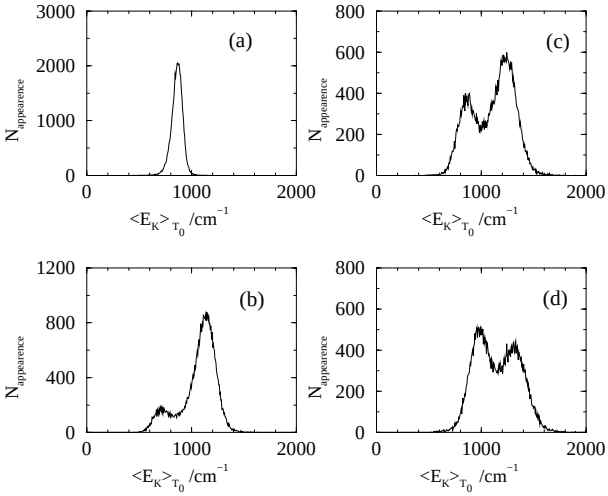

Fig. 2. Number of appearance of a given value of the time-averaged kinetic energy $\langle E_k \rangle_{T_0}$ in the case of the tetramer $(CH_3CN)_4$ at four different internal energies for which the kinetic temperatures are equal to: (a) $T = 136$ K; (b) $T = 155$ K; (c) $T = 165$ K; (d) $T = 169$ K. T_0 was equal to 1 ps.

As pointed out before with the analysis of the quenching trajectories, a less stable isomer ($E = -6\,662$ cm^{-1}) in the $(CH_3CN)_4$ cluster seems to play an important role in the dynamics. Thus the distribution of the time averaged kinetic energy $\langle E_k \rangle_{T_0}$ (calculated over $T_0 = 1$ ps) has been analysed for kinetic temperatures around the melting temperature of 153 K. Distributions of short time averaged kinetic energy are plotted in Figure 2. For a lower temperature than the melting temperature, only one peak appears which indicates that the cluster just vibrates around the equilibrium geometry associated with the minimum energy configuration. On the other hand, two peaks can

be clearly seen for the three temperatures $T = 155$, 165 and 169 K which are higher than the melting temperature. This indicates the coexistence of two isomers (or class of isomers) in the time window equal to $T_0 = 1$ ps. This dynamical coexistence can be seen as a phase coexistence in the sense that a dynamical coexistence between a hot solid (most stable isomer with a high mean kinetic energy) and a cold liquid (metastable isomer with a lower mean kinetic energy) can occur.

To test the number of isomers involved in this mechanism, we have run quenching trajectories for which the initial energy was slightly larger than the energy necessary for inducing the isomerization dynamics. Along this trajectory, only the two most stable isomers (S_4 and D_{2d}) have been found and the system spent 25% of the total duration in the metastable isomer D_{2d}. The difference of mean kinetic energy between the two peaks is equal to about 400 cm^{-1} which is larger than the difference of binding energies between the two most stable isomers in the $(CH_3CN)_4$ cluster [=234 cm^{-1}]. This larger value has to be due to anharmonic effects whose magnitude are different in the two regions of the PES. From a theoretical analysis of the vibrational shift of the CH_3 rock mode in the $(CH_3CN)_4$ cluster, Siebers *et al.* [22] have shown that only the S_4 geometry contributes to a red shift with respect to the monomer mode ($\nu_7 = 1\,041.8$ cm^{-1}). In particular, they have been able to explain the spectroscopic differences occurring in the IR-photodissociation spectra between the free $(CH_3CN)_4$ cluster [11] and the $(CH_3CN)_4$ embedded in helium clusters [13], the S_4 geometry being much more favorable in the $(CH_3CN)_4$ in helium clusters than in the free $(CH_3CN)_4$ cluster.

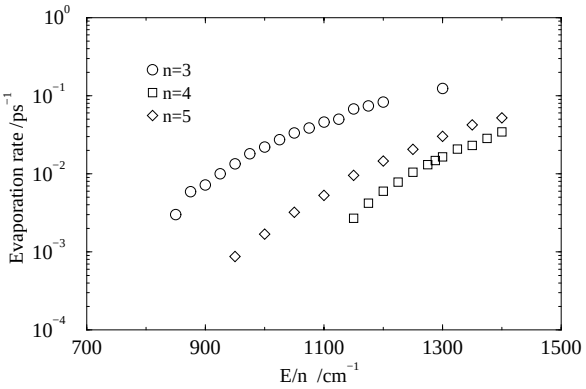

Fig. 3. Plot of the unimolecular evaporation rate as a function of E/n in the case of the parent molecular cluster $(CH_3CN)_n$ with $n = 3$, 4 and 5.

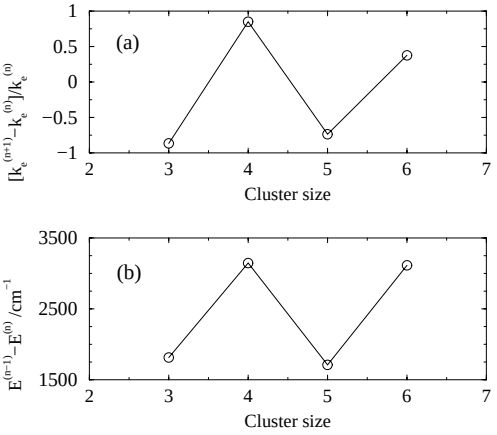

Fig. 4. (a) Evolution of the undimensional ratio $(k_e^{(n+1)} - k_e^{(n)})/k_e^{(n)}$ *versus* the cluster size n for $E/n = 1\,300$ cm^{-1}, $k_e^{(n)}$ and $k_e^{(n+1)}$ being respectively the evaporation rates of the $(CH_3CN)_n$ and $(CH_3CN)_{n+1}$ clusters; (b) evolution of the difference between the binding energies of the $(CH_3CN)_n$ and $(CH_3CN)_{n-1}$ clusters *versus* the cluster size n.

3.2 Evaporation process

Due to the strong electrostatic interaction between the polar acetonitrile molecules, the evaporation dynamics attempts to display some specific effects. In particular the dissociation of dimers from the parent clusters should be an efficient process in the energy range for which the MD simulations can be run.

3.2.1 Monomer evaporation

First of all, the dissociation dynamics of a monomer from the three parent clusters $n = 3$, 4 and 5 has been analysed as a function of the energy. In Figure 3 the evaporation rates are reported for these three cluster sizes. Due to the odd/even character of the number of molecules, a strong effect can be clearly evidenced. For a given internal energy per molecule E/n value, the evaporation rate constant of the $n = 4$ cluster is always lower than for $n = 3$ or 5. This clearly indicates that a cluster with an even number of CH_3CN molecules is more resistant with respect to dissociation due to its tendency to form dimer molecules inside the cluster.

For $E/n = 1\,300$ cm^{-1}, the evaporation rates have been calculated from $n = 3$ to $n = 7$. We note $k_e^{(n)}$ and $k_e^{(n+1)}$ respectively as the evaporation rates for the $(CH_3CN)_n$ and $(CH_3CN)_{n+1}$ parent clusters. In Figure 4a the ratio $[k_e^{(n+1)} - k_e^{(n)}]/k_e^{(n)}$ has been plotted as a function of n at the same internal energy per molecule E/n. The general trend for such a curve is that $k_e^{(n+1)} < k_e^{(n)}$, consequently negative values are generally obtained for the ratio previously defined. Figure 4a clearly shows an alternation between positive and negative values which demonstrates that the evaporation rate for an even number of molecules, $k_e^{(2n)}$, is thus lower than $k_e^{(2n-1)}$. This behaviour can be related to the evolution of the binding energies plotted in Figure 4b. The direct consequence of such an evolution of the evaporation rate as a function of the cluster size is that the cluster population in a typical mass spectrum will be larger for an even number of molecules. It has to be noted that the same behaviour has been observed for the pure Ar_n clusters in which the magic number $n = 13$ (icosahedral structure) is characterized by

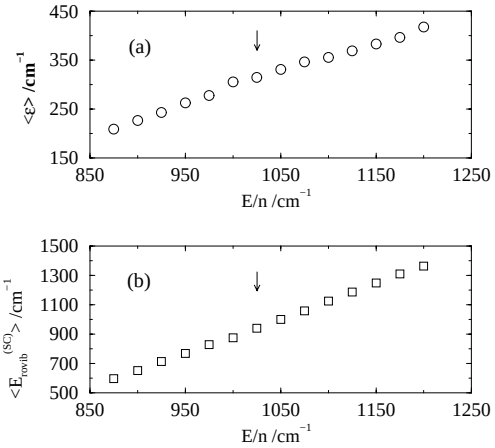

Fig. 5. (a) Ensemble averaged kinetic energy release as a function of E/n for the parent $(CH_3CN)_3$ cluster; (b) ensemble averaged rovibrational energy let in the dimer as a function of E/n.

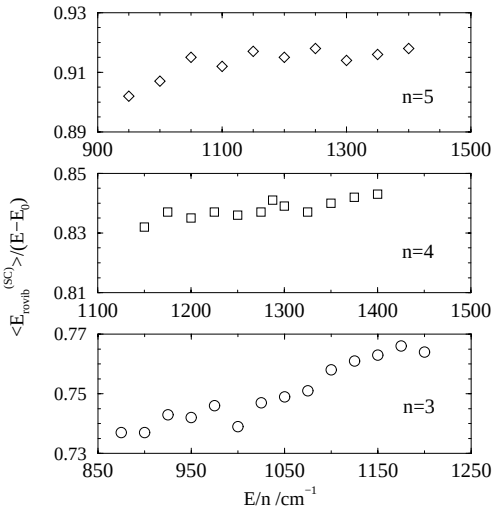

Fig. 6. Fraction of the rovibrational energy let in the $(CH_3CN)_{n-1}$ sub-cluster with respect to the internal energy injected in the parent $(CH_3CN)_n$ cluster.

a smaller rate constant than its nearest neighbours $n = 12$ and $n = 14$ [29].

Information on the energetics of the loss of a monomer from the parent cluster will be now discussed. Consider first the monomer evaporation of the $(CH_3CN)_3$ parent cluster for which only one dissociative channel is present $[(CH_3CN)_3 \rightarrow (CH_3CN)_2 + CH_3CN]$. In Figure 5a the evolution of the mean total kinetic energy release $\langle\epsilon\rangle$ $(= \epsilon_{\rm rot}^{(1)} + \epsilon_{\rm tr}^{(1)})$ in the unimolecular evaporation is reported as a function of the energy per molecule E/n. Around $E/n = 1\,000$ cm^{-1}, a change in the slope of this curve can be seen. In Figure 5b the evolution of the internal vibrational energy left in the sub-cluster $(CH_3CN)_2$ following the evaporation is reported. From the two curves, the change in the slope for the total kinetic energy release (*TKER*) takes place when the vibrational energy in the dimer is equal to around 900 cm^{-1}.

The analysis of the isomerization dynamics of the $(CH_3CN)_2$ dimer (not shown here) has revealed an increase of the δ parameter when the internal energy was about 950 cm^{-1}. Consequently, the evolution of the total kinetic energy release as a function of the internal energy in the parent cluster is altered by the change in the dynamics of the product dimer cluster. From a statistical point of view, this change in the slope can be related with the strong change of the density of states in the **product** cluster. Indeed, in the Phase Space Theory framework, it has been shown that the mean *TKER* can be written as:

$$\langle\epsilon\rangle = \frac{\int_o^{E-E_0} \epsilon f(\epsilon)\omega_{\rm p}(E - E_0 - \epsilon){\rm d}\epsilon}{\int_o^{E-E_0} f(\epsilon)\omega_{\rm p}(E - E_0 - \epsilon){\rm d}\epsilon}. \quad (5)$$

In this equation, E_0 is the difference between the binding energies of the most stable isomers of the parent and product clusters. $\omega_{\rm p}$ corresponds to the vibrational density of states in the product cluster. The function $f(\epsilon)$ can be evaluated by taking into account the constraints induced by the conservation of energy and angular momentum in the dissociation [39]. It has to be noted that equation (7) is correct only when the dissociation of the molecular cluster takes place without any potential barrier along the dissociative path (loose state theory).

Due to the link between $\langle\epsilon\rangle$ and the vibrational density of states $\omega_{\rm p}$ of the product cluster and due to the fact that $\omega_{\rm p}$ is altered around the solid-liquid like transition, the *TKER* evolution can be sensitive to the solid/liquid transition in the sub-cluster. This phenomenon had been already predicted in the case of the pure atomic Ar_n clusters [29] and had also been clearly observed from MD simulations in the case of the molecular clusters aniline-Ar_n [34] and inhomogeneous atomic clusters [30].

The energy sharing between the relative translation and the rotation of the evaporated molecule has been also analysed. For all the energies considered in this study, the evaporating molecule always has a larger amount of energy in the rotational degree of freedom than in the relative translational energy. The mean rotational energy is approximatively 30% larger than the mean relative translational energy. This gives evidence of the relative strong rotational energy excitation compared to the translational one which can be related to the rotational reorganization of the cluster in the dissociation dynamics.

As stated before, the change in the evolution of the *TKER* is a direct consequence of the entropic effects in such clusters. Some anharmonic effects in the sharing of the internal energy in the evaporation process can be also clearly seen when we plot the fraction of the rovibrational energy of the $(CH_3CN)_{n-1}$ sub-cluster with respect to the internal vibrational energy in the parent non-rotating $(CH_3CN)_n$ cluster. These curves have been plotted in Figure 6 in the case of the monomer evaporation from the parent clusters $n = 3$, 4 and 5. Systematically, the proportion of the mean rovibrational energy in the sub-cluster is increasing as a function of E/n which indicates that the harmonic description is not at all realistic in such systems. For $n = 3$, the strong increase of

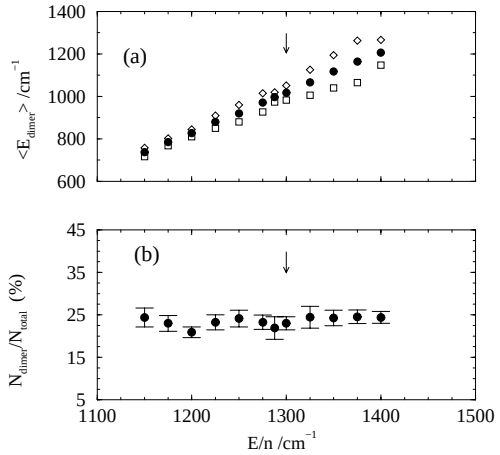

Fig. 7. (a) Ensemble-averaged vibrational energy of the dimers following the dissociation of the $(CH_3CN)_4$ in two dimers. Open squares and diamonds correspond to the energy of individual dimers. The filled circles correspond to the averaged energy of the two dimers; (b) fraction of evaporated dimers as a function of the internal energy per molecule E/n.

$E^{(SC)}_{rovib}/(E - E_0)$ near $E/n = 1\,000$ cm^{-1} is linked to the melting of the $(CH_3CN)_2$ product, as discussed previously. A similar effect can be evidenced for $n = 5$ (upper panel) where $E^{(SC)}_{rovib}/(E - E_0)$ begins to decrease for $E/n = 950$ and $1\,000$ cm^{-1}. For $n = 4$, no strong effect appears in the considered energy range because the melting of the product $(CH_3CN)_3$ is at very low temperature ($T = 28$ K). Consequently, MD simulations should be run at lower energy for which evaporative times should not be too long.

3.2.2 Dimer evaporation

Now we are going to analyse the dimer evaporation channel for the parent clusters $n = 4$ and 5. In Figure 7a, the mean rovibrational energy of the two $(CH_3CN)_2$ clusters following the dissociation of the parent cluster $(CH_3CN)_4$ has been reported. The open squares and the open diamonds correspond respectively to the mean rovibrational energy of the first and the second cluster detected in the simulation (with the geometrical criterium defined in the previous section). As the centers of mass of these two clusters are naturally at the same distance from the center of mass of the whole system, the first detected cluster will in fact have a generally larger distance between the two molecules inside this cluster. This explains why its mean internal energy is larger than the second one. The filled circles correspond to the averaged value for the rovibrational energy of the two dimers.

One interesting point to note is that, around 950–$1\,000$ cm^{-1}, the two mean values have a tendency to be even more different. In fact, this is the direct consequence of the solid-liquid like transition in the $n = 2$ cluster. Indeed when one dimer tends to take more vibrational energy, the second dimer tends to take a lower amount of energy due to the interaction between the two dimers along the reaction coordinate. Consequently, the mean vibrational energy for the two dimers (filled circle in Fig. 7a) is now almost linear *versus* E/n. This appears to be a notable difference with the situation of the monomer dissociation in which the energy conservation induces directly a decrease of the energy in the external degrees of freedom when the rovibrational energy of the sub-cluster increases. Thus the translational energy of the molecular fragments will be less sensitive to the solid-liquid like transition in the dimer evaporation compared to the monomer loss channel.

As seen just before, a characterization of the phase transition in the clusters is not really possible from the analysis of the *TKER* in the dimer evaporation dynamics. One other possibility could be the analysis of this phenomenon from the analysis of the fraction of ejected dimer in the dissociative events as a function of the energy. In Figure 7b, the dimer fraction is plotted as a function of E/n in the case of the dissociation of the $(CH_3CN)_4$ cluster. It appears that, in the energy range considered in this study, the dimer fraction is almost constant at around 25%. For the dissociation of the tetramer, the two dissociative channels have almost the same energy. The energy difference between the two asymptotic limits is equal to 121 cm^{-1}. The melting of the dimer occurs when the vibrational energy is equal to about 950 cm^{-1}, which corresponds to an internal energy per molecule in the parent cluster E/n of about $1\,275$ cm^{-1}. This is indicated by the arrow on the figure. Unfortunately no clear effect on the branching ratio can be evidenced at around this energy.

The lack of sensitivity of the dimer fraction to the solid-liquid like transition in the product cluster $(CH_3CN)_2$ is certainly due to the fact that the appearance of the solid-liquid transition in the product $(CH_3CN)_2$ cluster has no effect on the external degrees of freedom (see previous discussion). Consequently, the thermodynamical change does not really affect the dynamics of the dissociation and thus the branching ratio. One alternative explanation could be the presence of a potential barrier in the exit channel which means that the transition state can not be considered as the product cluster (loose state theory).

In Figure 8a, the dimer fraction has been plotted as a function of E/n but now in the case of the dissociation of the pentamer $(CH_3CN)_5$ cluster. In this case there is a large energy difference between the two exit channels, *i.e.* the $(CH_3CN)_3 + (CH_3CN)_2$ energy is $1\,210$ cm^{-1} higher than the $(CH_3CN)_4 + (CH_3CN)_1$ energy. The analysis of Figure 8a shows a different behaviour than in the case of $(CH_3CN)_4$ evaporation. Now, the branching ratio is strongly dependent on the internal energy in the parent cluster. In the energy range considered in the *MD* simulations, the branching ratio evolves from 10 to about 30%.

If we make the assumption that the evolution of the dimer fraction is a monotonic function *versus* E/n, it is possible to determine if the dimer evaporation is governed by a potential barrier in the exit channel by extrapolating this curve to zero. Following this procedure, we find that the branching ratio tends to zero when E/n is equal to

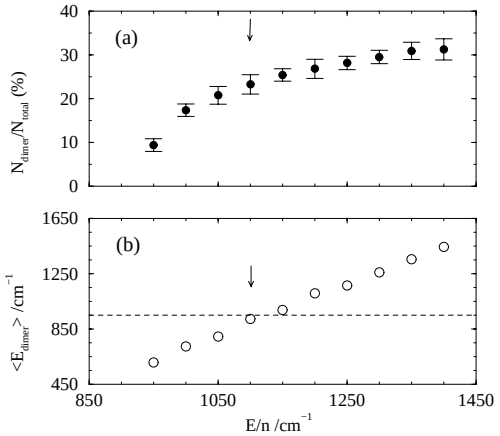

Fig. 8. (a) Fraction of evaporated dimers as a function of the internal energy per molecule E/n for the dissociative process $(CH_3CN)_5 \rightarrow (CH_3CN)_3 + (CH_3CN)_2$; (b) ensemble-averaged vibrational energy of the dimer following the same dissociative process.

about (850 ± 50) cm^{-1}. From this approximate value, we could conclude that the dynamics is governed by a large energy barrier $E_b = (1\,330 \pm 250)$ cm^{-1} which could be understood by an angular reorganization along the dissociative path in the PES due to the strong dipole-dipole electrostatic interaction. The presence of this barrier could explain the lack of sensitivity of the branching ratio to the solid-liquid transition in the product $(CH_3CN)_2$ dimer which should appear at $E/n \approx 1\,100$ cm^{-1} (see the arrow in Fig. 8) when the mean rovibrational energy $\langle E_{dimer} \rangle$ in the dimer is approximatively equal to 950 cm^{-1} (see Fig. 8b). However the energy barrier found previously seems too high for such a molecular cluster.

A more convincing explanation can now be mentioned. Up to now, we have only considered the solid-liquid like phase transition in the $(CH_3CN)_2$ dimer in the exit channel $(CH_3CN)_5 \rightarrow (CH_3CN)_3 + (CH_3CN)_2$. In the second channel involving the loss of a monomer, a phase transition also occurs in the product molecular cluster $(CH_3CN)_4$ when $E/n \approx 825$ cm^{-1}. This value is easily derived from the knowledge of the temperature ($T = 153$ K) associated with the solid-liquid transition in this cluster (see Tab. 2) and from information (obtained from MD simulations) on energy shared between all the degrees of freedom (see Fig. 6). As explained before, in the case of a monomer ejection, the external mean kinetic energy of the fragments will be sensitive to the phase transition. Thus the branching ratio is also sensitive and can be modified around $E/n \approx 825$ cm^{-1}. Consequently, the branching ratio may be not at all a monotonic function in this range of energy. The lowering of the dimer fraction obtained from MD simulations near $E/n = 950$ cm^{-1} is certainly a consequence of the strong change in the entropy function for the tetramer. As discussed previously, a dynamical phase coexistence has been clearly put into evidence (see Fig. 2) over a broad energy region which means that the effect on the branching ratio can still be seen around $E/n = 950$ cm^{-1} although the onset of this phenomenon must appear near $E/n = 825$ cm^{-1}. Unfortunately, MD simulations can not be directly run around this low energy value because the typical time of evaporation is too low.

4 Conclusion

A classical molecular dynamics simulation of the isomerization and evaporation dynamics in the free acetonitrile clusters has been reported. The analysis of the isomerization dynamics from long time simulations (50 ns) has confirmed the value of the solid-liquid transition temperature, previously calculated from canonical [25] and microcanonical [23] simulations. A strong dependence of these melting temperatures in acetonitrile clusters as a function of the cluster size has been clearly confirmed.

For the first time, the evaporation of a molecular cluster composed of strong polar molecules has been simulated. As expected, a large fraction of dimers is evaporated following the heating of the parent cluster. The influence of the phase transition in the product clusters on the energetics and dynamics in the evaporation process has been discussed. Although the influence on the kinetic energy release has been well established in the case of the monomer evaporation, this work has shown the difficulty in observing such a phenomenon for the dimer evaporation channel. This loss of sensitivity has been understood as the consequence of the potential coupling between the dimer and the sub-cluster at the first stage of the dissociation which induces an efficient energy transfer between the vibrational degrees of freedom of the two components. The kinetic energy release in the external degrees of freedom is thus less modified when the solid-liquid like phase transition occurs in the $(CH_3CN)_{n-2}$ or in the $(CH_3CN)_2$ products following the dissociation of the parent $(CH_3CN)_n$ cluster.

The competition between the monomer and the dimer evaporation has been carefully analysed as a function of the internal energy. In the case of the evaporation of the $(CH_3CN)_5$ cluster, a strong decrease in the dimer fraction is seen, which has been explained as the consequence of the melting of the $(CH_3CN)_4$ product cluster. From an experimental point of view, this could be tested by analysing the dimer fraction in an experimental set-up with a time of flight apparatus after injecting a given amount of energy into a mass-selected parent $(CH_3CN)_n^+$ ionic cluster. A change in the dimer fraction is expected to appear near the melting temperature associated with the $(CH_3CN)_{n-1}^+$ cluster. A statistical study within the PST formalism is in progress to confirm the effect of the solid-liquid like phase transition on the branching ratio.

References

1. H. Bertagnolli, P. Chieux, M.D. Zeidler, Mol. Phys. **32**, 759 (1976)
2. H. Bertagnolli, M.D. Zeidler, Mol. Phys. **35**, 177 (1978)
3. B.H. Torrie, B.M. Powell, Mol. Phys. **75**, 613 (1992)
4. E. Knozinger, D. Leutloff, J. Chem. Phys. **74**, 4812 (1981)

5. E. Knozinger, P. Beichert, J. Hemeling, O. Schrems, J. Phys. Chem. **97**, 1324 (1993)
6. W. Langel, H. Kollhoff, E. Knozinger, Ber. Bunsenges. Phys. Chem. **89**, 927 (1985)
7. A.S. Al Mubarak, G. Del Mistro, P.G. Lethbridge, N.Y. Abul-Sattar, A.J. Stace, Faraday Discuss. Chem. Soc. **86**, 209 (1988)
8. U. Buck, H. Meyer, J. Chem. Phys. **84**, 4854 (1986)
9. M.H. Mengel, G. Scoles, in *The chemical physics of atomic and molecular clusters* (CVII Enrico Fermi School, Varenna, 1988)
10. D.J. Levandier, M. Mengel, J. McCombie, G. Scoles, *The chemical physics of atomic and molecular clusters*, edited by G. Scoles (North-Holland, Amsterdam, 1990), p. 331
11. U. Buck, X.J. Gu, R. Krohne, Ch. Lauenstein, Chem. Phys. Lett. **174**, 247 (1990)
12. U. Buck, I. Ettischer, Faraday Discuss. Chem. Soc. **97**, 215 (1994)
13. M. Behrens, R. Frochtenicht, M. Hartmann, J.G. Siebers, U. Buck, F. Hagemeister, J. Chem. Phys. **111**, 2436 (1999)
14. C. Desfrancois, H. Abdoul-Carime, N. Kheila, J.P. Schermann, V. Brenner, P. Millie, J. Chem. Phys. **102**, 3791 (1994)
15. M.W. Evans, J. Mol. Liq. **25**, 149 (1983)
16. H.J. Böhm, I.R. Mc Donald, P.A. Madden, Mol. Phys. **49**, 347 (1983)
17. P.A. Steiner, W. Gordy, J. Mol. Spectrosc. **21**, 291 (1966)
18. W.L. Jorgensen, J.M. Briggs, Mol. Phys. **63**, 547 (1988)
19. D. Mathieu, M. Defranceschi, J. Delhalle, Int. J. Quant. Chem. **45**, 735 (1993)
20. M. Defranceschi, D. Peters, D. Mathieu, J. Delhalle, G. Lécayon, J. Mol. Struct. (Theochem) **287**, 153 (1993)
21. M. Bertolus, V. Brenner, P. Millie, J.B. Maillet, Z. Phys. D **39**, 239 (1997)
22. J.G. Siebers, U. Buck, T.A. Beu, Chem. Phys. **239**, 549 (1998)
23. G. Del Mistro, A.J. Stace, J. Chem. Phys. **99**, 4656 (1993)
24. A.J. Stace, G. Del Mistro, J. Chem. Phys. **102**, 5900 (1995)
25. D. Wright, M.S. El-Shall, J. Chem. Phys. **100**, 3791 (1994)
26. C.E. Roman, I.L. Garzon, Z. Phys. D **20**, 163 (1991)
27. R.W. Smith, Z. Phys. D **21**, 57 (1991)
28. C. Rey, L.J. Gallego, M.P. Iniguez, J.A. Alonso, Physica B **179**, 273 (1992)
29. S. Weerasinghe, F.G. Amar, Z. Phys. D **20**, 167 (1991); S. Weerasinghe, F.G. Amar, J. Chem. Phys. **98**, 4967 (1993)
30. P. Parneix, Ph. Bréchignac, J. Chem. Phys. (accepted)
31. R.N. Barnett, U. Landman, G. Rajagopal, Phys. Rev. Lett. **67**, 3058 (1991)
32. M.J. Lopez, J. Jellinek, Phys. Rev. A **50**, 1445 (1994)
33. G.H. Peslherbe, W. Hase, J. Chem. Phys. **105**, 7432 (1996)
34. P. Parneix, Ph. Bréchignac, F.G. Amar, J. Chem. Phys. **104**, 983 (1996)
35. P. Parneix, F.G. Amar, Ph. Bréchignac, Chem. Phys. **239**, 121 (1998)
36. F. Calvo, J. Phys. Chem. B **105**, 2183 (2001)
37. P. Pechukas, J.C. Light, J. Chem. Phys. **42**, 3281 (1965)
38. D.J. Evans, Mol. Phys. **34**, 317 (1977); D.J. Evans, S. Murad, Mol. Phys. **34**, 327 (1977)
39. W.J. Chesnavich, M.T. Bowers, J. Chem. Phys. **66**, 2306 (1977)